SPE-189886-MS

Measurements While Fracturing: Nonintrusive Method of Hydraulic Fracturing Monitoring

S. Parkhonyuk, A. Fedorov, A. Kabannik, R. Korkin, M. Nikolaev, and I. Tsygulev, Schlumberger

This paper was prepared for presentation at the SPE Hydraulic Fracturing Technology Conference & Exhibition held in The Woodlands, Texas, USA, 23-25 January 2018.

Abstract

A new method of nonintrusive fracturing process monitoring in real time has been developed. The method is a combination of advanced signal processing algorithms and a tube wave velocity model based on Bayesian statistics and, thus, does not require complex hardware. This enables cost-effective and timely decisions at the wellsite. The technique was validated in the field in several fracturing and refracturing jobs.

Introduction

A new method of real-time hydraulic fracturing monitoring has been developed. The method uses data that are already routinely collected during such operations and allows overcoming the common issue of downhole completion underperformance in hydraulically fractured wells. Events that can diminish the effectiveness of multistage fracturing include fracturing ports not opening because of ball landing failure and failure of isolation packers such as bridge plugs to divide the horizontal section into several subzones, among others. Several monitoring methods exist, including microseismic monitoring, heterodyne distributed vibration sensing (hDVS), distributed temperature sensing (DTS), traceable proppant, and chemical tracers. However, these methods may be cost prohibitive, and they provide results only after the job is completed. The necessity of nonintrusive real-time monitoring of the fracturing process and the lack of possibility to deploy expensive methods at all jobs spurred the development of the proposed technique, which allows proactive changes on the wellsite to ensure proper wellbore coverage and to avoid overstimulation of one interval/cluster and understimulation of another zone.

Treating pressure is the first parameter that is recorded during hydraulic fracturing. Pressure oscillations recorded during the pumps shutdown are known as water hammers. Pressure behavior is used to estimate reservoir parameters and water hammers are used for the estimation of near-wellbore restrictions. The water hammers are caused by tube waves traveling in the wellbore from the surface down hole, reflecting off the completion elements (end of tube, fracture, tube enlargement, or a combination of all of these), and traveling back. Usually, it is possible to detect a few cycles before full attenuation of such waves. If these data are recorded with the required sampling rate (typically above few tens of Hertz), then the water hammer signal can be reconstructed with an accuracy sufficient to determine the signal period (i.e., the time required for a tube wave to travel from surface to an reflector and back). The fundamentals of hydraulic fracture

characterization by surface pressure oscillation analysis were initially outlined in (Holzhausen and Gooch 1985). Recent advances in application of the technique related to leak isolation detection are reported in (Bogdan et al. 2016).

The method of hydraulic fracturing monitoring presented in this paper is called measurements while fracturing (MWF). It is characterized by enhanced event detectability and higher reflection depth determination accuracy. These are achieved by a combination of advanced signal processing algorithms and a tube wave velocity model based on Bayesian statistics, where each new signal is used as posterior information for decreasing uncertainty.

The method is applicable to wells completed with cemented liner (plug and perf) and sliding sleeves and in refracturing jobs with some modifications. Although in some stages the method has been successfully benchmarked against microseismic data or DTS, the full-scale benchmarking (i.e., for all stages of multistage wells) is still expected.

A typical well sketch is shown in Fig. 1. A horizontal section may contain as many as 30 to 40 stimulated stages. The distance between them may be 150 to 300 ft. The goal of such multiple stimulation is production intensification. To achieve that, all stages should be separated, either by chemical diverters or by mechanical plugs, such as balls, which must be settled to specially designed saddles. These methods of wellbore isolation allow fluid to be pumped into newly created perforation intervals. However, the chemical diverters might not fully plug the previously stimulated stages, and balls may cause leakage or may be damaged during landing. In these cases, fluid will be pumped to already stimulated stages, making the job inefficient. Timely detection of such an event allows the operator to take actions for optimal well stimulation, for example, remedial plugging of a given interval, changing chemical diverter type, etc. Such operation should be performed in real time or almost real time to achieve efficient well stimulation.

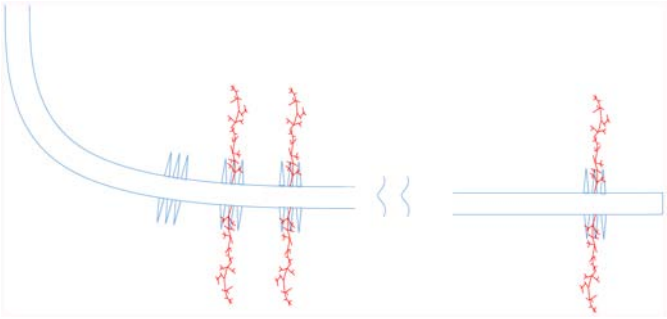

Figure 1—A horizontal section of a stimulated well. The section may have 30 to 40 stages (with one fracture per stage).

The suggested algorithm for stimulation efficiency evaluation is divided into two steps: detection of echoes in pressure signals followed by reflection depth determination with the tube wave velocity model. These steps are described in the next two sections.

Cepstrum Analysis

The surface pressure signal $y(t)$ can be represented as a sum of useful signal $x(t)$ and noise component $e(t)$:

$$y(t) = x(t) + e(t) \tag{1}$$

The noise component $e(t)$ contains broadband electronic noise, narrow harmonic peaks caused by hydraulic pump strokes, and a zero-frequency trend component related to the slow treatment pressure variations. The bandwidth of the useful signal $x(t)$ is limited in the frequency interval from approximately 0.1 Hz to approximately 15 to 20 Hz depending on the pump shutdown time and hydraulic signal attenuation in the wellbore. Therefore, at the preprocessing stage, the filter should be applied to the surface pressure signal $y(t)$, which preserves the useful signal $x(t)$ within its bandwidth and discards the noise $e(t)$.

The noise $e(t)$ is removed from the signal at the preprocessing stage by application of Gaussian derivative bandpass filter that removes both zero-frequency and high-frequency components of the signal.

Similarly to the convolution model of a recorded seismogram (Yilmaz 2001), the useful signal $x(t)$ can be represented as the convolution of the source pressure pulse $s(t)$ excited by the water hammer and wellbore reflectivity $w(t)$:

$$x(t) = s(t) * w(t) \tag{2}$$

The wellbore reflectivity $w(t)$ is the unknown parameter in the convolution equation (Eq. 2). Normally, it is a decaying minimum-phase train of echo pulses delayed by pressure pulse oscillation periods T and the pulse amplitudes a depend on the corresponding reflection coefficients and wave attenuation in the wellbore:

$$w(t) = \delta(t) + \sum_{k=1}^{+\infty} a^k \delta(t - kT) \tag{3}$$

where $0 < |a| < 1$ and $\delta(t)$ is a unit pulse:

$$\delta(t) = \begin{cases} 1, t = 0 \\ 0, t \neq 0 \end{cases}$$

The reflection coefficients are determined by hydraulic impedance changes at the reflection boundaries. For hydraulic fractures, they are negative and for wellbore restrictions they are positive (Holzhausen and Gooch 1985).

To estimate the unknown wellbore reflectivity $w(t)$ from the convolution equation (Eq. 2), the cepstrum algorithm is applied. The cepstrum is a nonlinear signal processing technique. It was introduced by (Bogert et al. 1963) and originally was used for characterizing the seismic echoes resulting from earthquakes and bomb explosions. They also introduced a terminology: the term "cepstrum" is derived by reversing the first four letters of "spectrum". Similarly, the name of the independent variable τ is known as a "quefrency" and it has the dimension of time.

The cepstrum is the result of taking the inverse Fourier transform of the logarithm of the estimated spectrum of a signal:

$$\hat{x}(\tau) = \frac{1}{2\pi} \int log\left[\left|\int x(t) e^{i\omega t} dt\right|\right] e^{-i\omega\tau} d\omega \tag{4}$$

The presence of logarithm in (Eq. 4) allows separating the useful signal $x(t)$ into two parts in the cepstral domain:

$$\hat{x}(\tau) = \hat{s}(\tau) + \hat{w}(\tau) \tag{5}$$

where $\hat{s}(\tau)$ and $\hat{w}(\tau)$ are cepstra of the source signal and wellbore reflectivity. The cepstrum of wellbore reflectivity $w(t)$ defined in (Eq. 3), which is a train of delayed echoes, will also be a train of delayed echoes:

$$\hat{w}(\tau) = \sum_{k=1}^{+\infty} \frac{a^k}{k} \delta(\tau - Tk) \tag{6}$$

The pressure pulse caused by pump shutdown $s(t)$ has a smooth spectrum, and therefore its cepstrum $\hat{s}(\tau)$ is located around low quefrency values (Tribolet and Oppenheim 1977) that can be easily separated from the wellbore reflectivity response $\hat{w}(\tau)$ in the cepstral domain, which has non-zero peaks only at quefrencies of T, $2T$, $3T$,…

According to present method, the cepstrogram is computed; the cepstrogram is a visual representation of the cepstrum of the pressure data as it varies in time. The wellbore pressure oscillations caused by tube wave reflections from hydraulic fractures are manifested by strong negative peaks on the cepstrogram at appropriate quefrencies. Similarly, the wellbore pressure oscillations caused by tube wave reflections from wellbore restrictions result in strong positive peaks on the cepstrogram.

An example of the water hammer and corresponding cepstrogram is shown in Fig. The strong negative peaks on the cepstrogram indicate reflection from the fracture. The traced quefrencies (in white) correspond to oscillation period of 7.09 s.

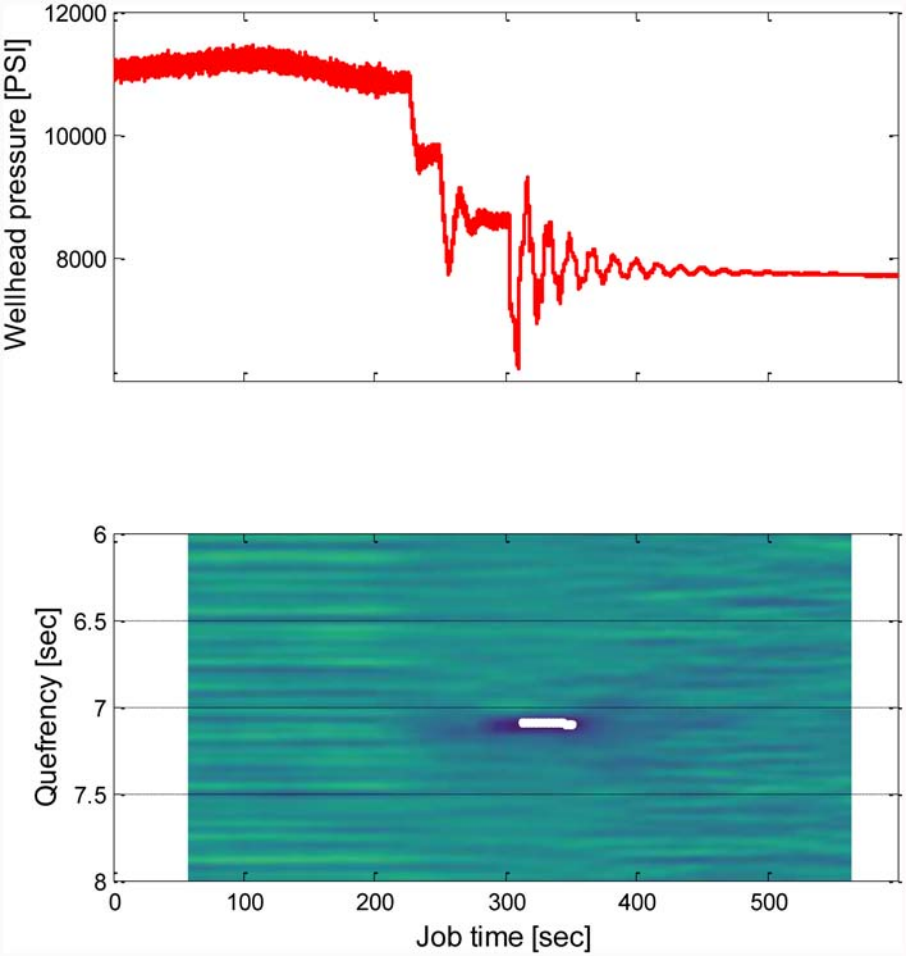

Figure 2—Pressure oscillations during water hammer and the cepstrogram plotted in quefrency vs. time. The strong negative peaks on the cepstrogram indicate reflection from the fracture. The traced quefrencies (in white) correspond to an oscillation period of 7.09 s.

Velocity Computation

The next step is to convert time to depth. The tube wave velocity plays the role of a conversion coefficient. The general expression for tube wave velocity may be found in (Holzhausen and Lawrence 1986):

$$c = \sqrt{\frac{K_{eff}}{\rho}}, K_{eff}^{-1} = K^{-1} + \left(G + E\frac{t}{D}\right)^{-1} \quad (7)$$

Here, H_{eff} is an effective bulk modulus; K and ρ are fluid bulk modulus and density, respectively; G is the surrounding formation shear modulus; E, t, and D are the casing shear modulus, thickness, and diameter, respectively. As it is seen, the tube wave velocity depends on many parameters: fluid properties, wellbore geometry and elastic properties, and formation parameters. Even the major contributor—fluid bulk modulus and density—depend significantly on pressure, temperature, air presence, and the wave's frequency. The sound wave velocity in pure water $c_w = \sqrt{\frac{K_w}{\rho_w}}$ varies from 5000 to 5400 ft/s for pressure changing from 2,000 to 10,000 psi (Wilson 1960). A comparable effect comes from temperature. Air presence causes a significant impact even at a very small amount of air. The tube wave velocity cannot be theoretically computed with

accuracy better than 300 to 400 ft/s. This uncertainty causes depth uncertainty (for typical quefrency, as in the example above, 7.09 s):

$$\Delta L = \Delta c\tau/2 \sim 1{,}000 - 1{,}500\ ft \tag{8}$$

This is inapplicable for practical purposes, because distance between the stages is 150 to 300 ft, as discussed above. Instead, the velocity of tube waves will be calculated in a few steps. The first event depth is usually known (at least in plug-and-perf cases); it is the first perforation depth. When the first interval stimulation is over and data are processed, the velocity can be computed. In addition, the algorithm determines velocity uncertainty, based on width of the perforation interval and quefrency uncertainty. These data allow predicting the depth of the second event when the second stimulation is over. Depending on the velocity accuracy and the second interval data, the algorithm determines the depth of the second stimulation and, as a result, whether the second interval is successfully stimulated (the pumping done into the second interval) or failed (pumping gone to the first interval) or at least the probabilities of each of those events. Then, the velocity is recalculated based on new data for each of the scenarios (and now is known with higher accuracy for each given scenario). Moreover, better knowledge of a velocity allows recomputing the first interval depth and its uncertainty based on the posterior information about this depth based on the velocity and quefrency. In a similar way, all events are processed, providing increasingly more accurate data on velocity and depths of already stimulated fractures. At the end of the job (or at the end of each interval) the algorithm provides one or few scenarios (arrays of information about where the pumping was done at each event) with their probabilities, which finally can be converted to a success/failure probability of the stimulation of each interval.

The real-time detection of a failed event allows taking additional actions, such as diverter pumping; the knowledge of a successfully performed stimulation allows proceeding with the job as designed. If the job efficiency is known only with some probability, then an extra data may be requested to draw a conclusion about the stimulation efficiency by generating a new water hammer. Thus, the operator is able to obtain real-time information about the fracturing process and use it for decision making. This allows saving thousand dollars by avoiding extra-diverter pumping and overstimulating already stimulated intervals. Instead, the careful information-based decision making allows optimizing the multistage hydraulic fracturing process, providing maximum well productivity at minimal time and cost.

Case Studies

The method described above was successfully applied in a 5.5-in. cased well in the Woodford basin. The horizontal well was landed in the Granite Wash formation with a 6,000-ft lateral. A plug-and-perf completion was performed with eight intervals of approximately 400 ft, each perforated by six clusters. The well was stimulated by crosslinked fluid with 40/70 white sand. Eight stages were pumped. On stages 2 through 8, diverter was used. On this job, a radioactive tracer was pumped with 40/70 sand on all intervals except stages 5 and 7. As the radioactive material, iridium, antimony, and scandium were used. On the same well, high-frequency pressure monitoring was performed for all intervals except for interval 5 due to technical issues.

The information on the tracer's distribution across the interval is very important because it provides a direct method of determining diversion efficiency. This method provides very good depth resolution; however, is expensive and does not allow acquiring data in real time. Therefore, the use of tracers is not applicable for real-time decisions. At the same time, a combination of two methods of evaluating the diversion efficiency provides excellent benchmarking of the efficiency of the MWF method. Fig. 3. Demonstrates locations of the detected tube wave events matched with radioactive tracer log. The color of each event match the color of radioactive tracer pumped during respective stage. The color intensity of the spots shows the probability of the fluid entry point determination, while the size indicates the depth

determination uncertainty. Table 1 summarizes the lateral lengths and the methods used at every interval. In this paper, only stages that were measured both by MWF and tracers are compared.

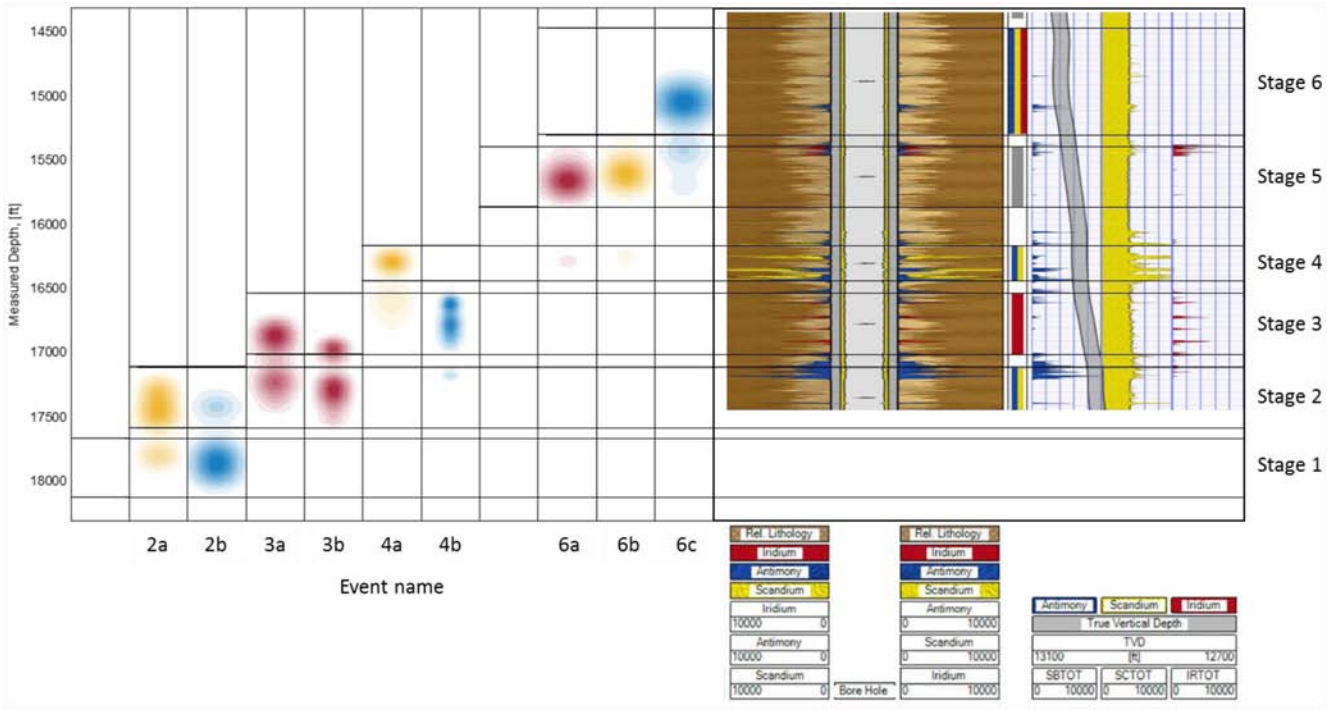

Figure 3—Locations of the detected tube wave events matched with radioactive tracer log. The color of each event match the color of radioactive tracer pumped during respective stage. The color intensity of the spots shows the probability of the fluid entry point determination, while the size indicates the depth determination uncertainty.

Table 1—Summary of the used methods and interval lengths.

Interval	Interval Length, ft	Diverter Used / Number of Fracturing Operations	Tracer	MWF
1	460	No / 1	No	No
2	478	Yes / 2	Yes	Yes
3	478	No / 2	Yes	Yes
4	274	Yes / 2	Yes	Yes
5	469	Yes / 1	No	No
6	822	Yes / 3	Yes	Yes
7	480	Yes / 2	No	Yes
8	420	Yes / 2	Yes	No

The results of MWF measurements showed no information about the stimulation of the first interval. The first pumping (ramp) of the second interval contained scandium tracers, which showed significant background over the entire wellbore, and thus it is hard to conclude if this pumping failed or not according to a tracer log. The second ramp contained antimony; because there is no tracer log of the first interval, it is hard to conclude whether all the fluid was pumped into the second interval or part of it to the first interval. Results from the MWF method (Fig. 4.) indicate that the first ramp was most likely successful (74%) and fluid was pumped to a second interval; the second pumping failed (67% probability). These percentage distributions cannot be clearly interpreted as probabilities only, but may reflect fluid pumping in different ratios (i.e., 67% distribution of successful stimulation may also mean that most of fluid was pumped into

designed interval and the rest was pumped into a previous one). The absence of tracer data from the first interval and the low confidence in the MWF data in the second interval do not allow us to conclude whether the MWF determined the stimulation efficiency of this interval correctly or not.

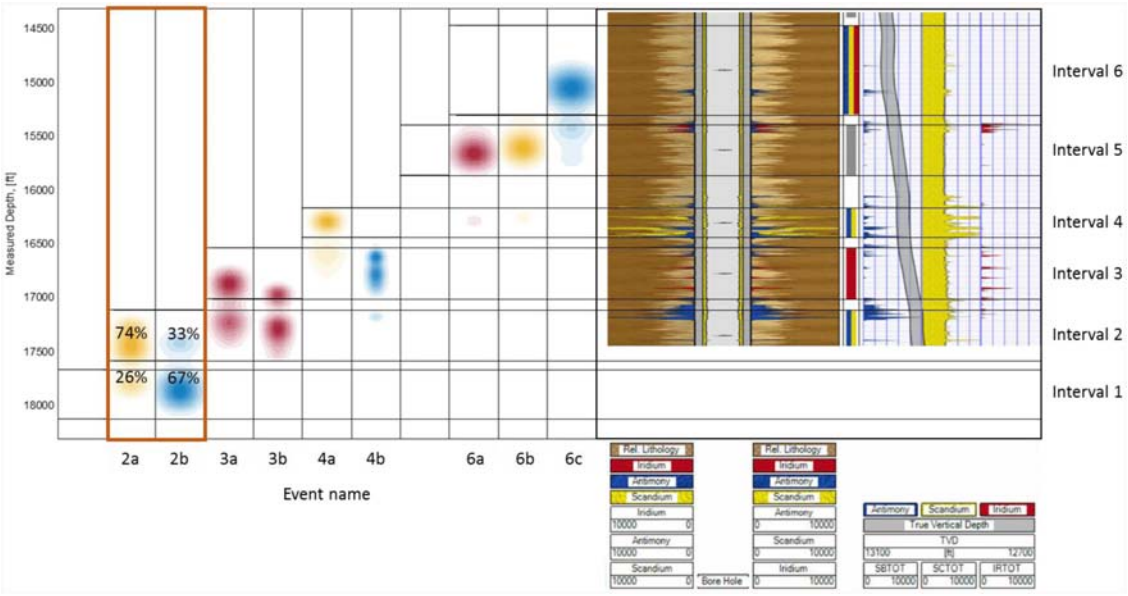

Figure 4—Probabilities of the fluid entry point determinations for interval 2 matched with the radioactive tracer log

The third interval also was pumped in two steps with the diverter between them, and it showed a 63% probability of success (Fig. 5) for the first ramp and approximately 50% probability of success/failure for the second ramp. As noted above, this may be caused by the fluid being pumped into both intervals (2 and 3) during this pumping. This is well confirmed by the tracers the amount of iridium (red) is comparably small in this interval, although some amount of iridium is observed in the second interval.

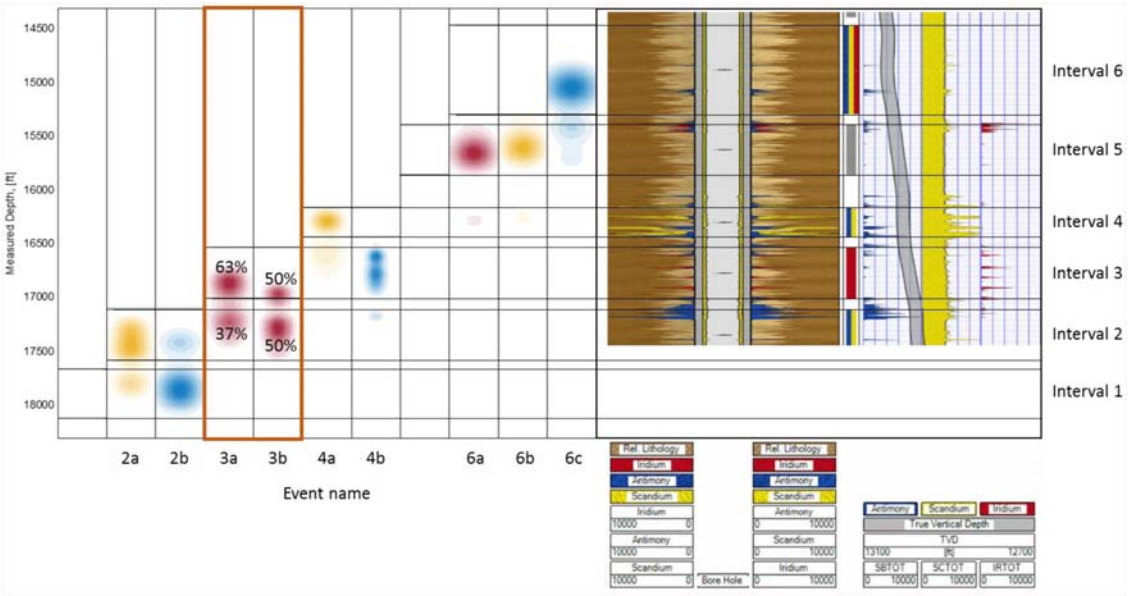

Figure 5—Probabilities of the fluid entry point determinations for interval 3 matched with the radioactive tracer log

The fourth interval had two ramps separated by diverters as it is shown in Fig. 6. The first one was done successfully (85%), and the second failed (92%). The tracer log confirms that some amount of antimony (blue) is observed in interval 3, where it was not pumped.

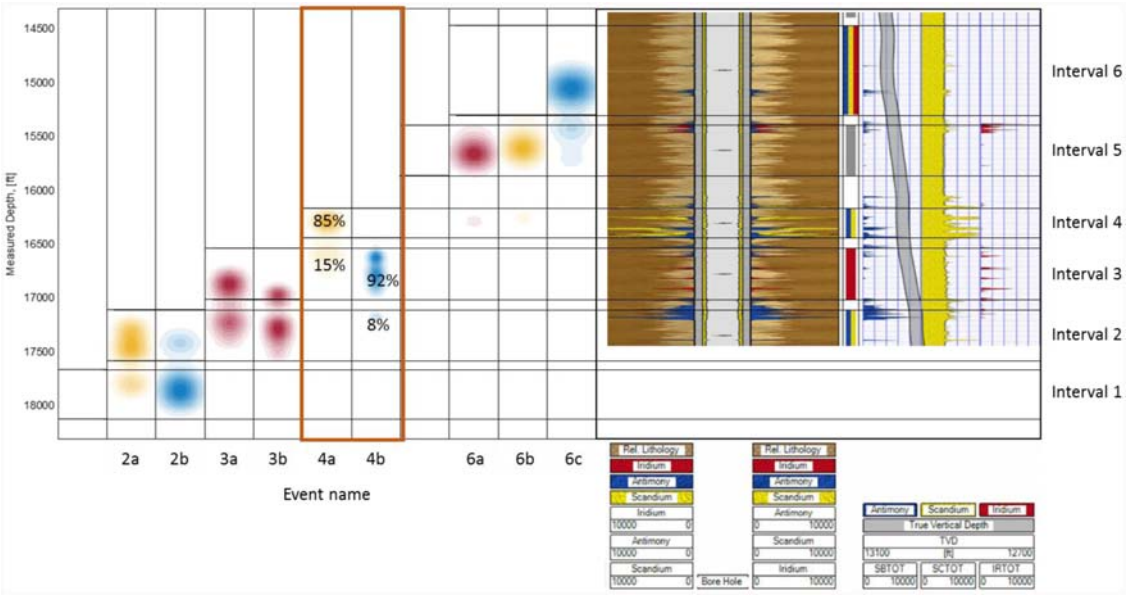

Figure 6—Probabilities of the fluid entry point determinations for interval 4 matched with the radioactive tracer log

Interval 6 was pumped in three ramps with diverters between them as it is shown in Fig. 7. The first two pumpings, which failed according to MWF data with 93 and 88% probabilities, contained iridium (red) and scandium (yellow), which were not observed in the log at all. The third ramp in interval 6, which was successful with 92% probability according to MWF data, contained antimony (blue), which is visible at the depth 15,100 ft. Therefore, both methods clearly indicate that the first two ramps failed and only the last one was done successfully.

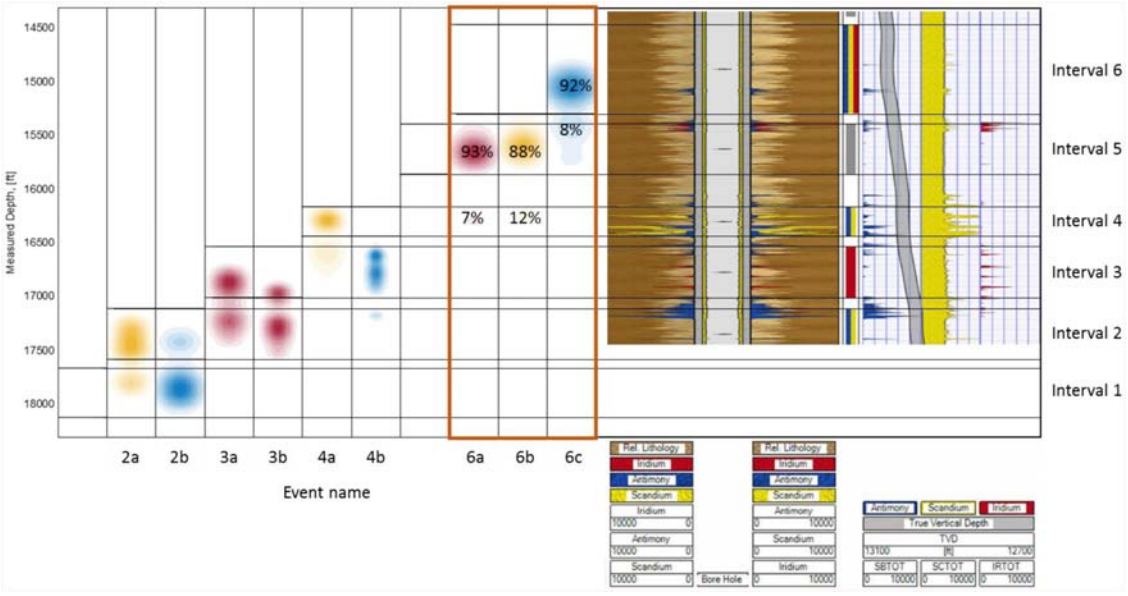

Figure 7—Probabilities of the fluid entry point determinations for interval 6 matched with the radioactive tracer log

Conclusion

The method discussed above describes how to determine the stimulation efficiency in a multistage hydraulically fractured well based on high-frequency pressure sensor data. The method allows real-time monitoring of the stimulation process and gives data that can be used in decision-making. It was successfully benchmarked with radioactive tracer data (full agreement between two methods). The depth coincidence between the two methods shows an error within 100 ft, which demonstrates the applicability of this method in most plug-and-perf cases where the space between intervals generally exceeds 140 ft). With minimal modifications, the method can be used in all other stimulation jobs (sliding sleeves, refracturing, etc.).

Compared to other methods of stimulation efficiency determination, the MWF method is cheap, nonintrusive, direct (i.e., fluid entry point determination usually determines fracture location), and, as mentioned above, provides real-time data.

References

Bogdan, A. V., Keilers, A., Oussoltsev, D. et al 2016. Real-Time Interpretation of Leak Isolation with Degradable Diverter Using High Frequency Pressure Monitoring. Presented at the SPE Asia Pacific Oil & Gas Conference and Exhibition, Perth, Australia, 25-27 October. SPE-182451-MS. https://doi.org/10.2118/182451-MS.

Bogert, B. P., Healy M. G., and Tukey J. W. 1963. The Quefrency Alanysis [sic] of Time Series for Echoes: Cepstrum, Pseudo Autocovariance, Cross-Cepstrum and Saphe Cracking. In *Proceedings of the Symposium on Time Series Analysis*, ed. Rosenblatt,M. chapter 15, 209–243. New York: John Wiley.

Holzhausen G.R. and Gooch R.P. 1985. Impedance of Hydraulic Fractures: Its Measurement and Use for Estimating Fracture Closure Pressure and Dimensions. Presented at the SPE/DOE Low Permeability Gas Reservoirs Symposium, Denver, Colorado, 19-22 March. SPE-13892-MS. https://doi.org/10.2118/13892-MS.

Holzhausen G. R. and Lawrence, W., St. 1986. Hydraulic Fracture Analysis Method. US Patent 4802144A.

Tribolet J. M. and Oppenheim A. V. 1977. Deconvolution of Seismic Data Using Homomorphic Filtering. Presented at the Joint Automatic Control Conference. San Francisco, California, USA.

Wilson W. D. 1960. Equation for the Speed of Sound in Sea Water. *J. Acoust. Soc. Amer*. **32** (10): 1357. https://doi.org/10.1121/1.1907913.

Yilmaz O. 2001. *Seismic Data Analysis: Processing, Inversion and Interpretation of Seismic Data*, ed. Doherty.S.M. Tulsa: Society of Exploration Geophysicists.